

# The Effect of Starting Precursors on Size and Shape Modification of ZrB<sub>2</sub> Ceramic Nanoparticles

Zahra Amirsardari<sup>1</sup>, Rouhollah Mehdinavaz Aghdam<sup>2,\*</sup>,  
Masoud Salavati-Niasari<sup>1</sup>, and Mohammad Reza Jahannama<sup>2</sup>

<sup>1</sup>Institute of Nano Science and Nano Technology, University of Kashan, Kashan, P.O. Box 87317-51167, I. R. Iran

<sup>2</sup>Department of Nano Technology, Space Transportation Research Institute, Tehran, P.O. Box 13445-75411, I. R. Iran

The formation of ZrB<sub>2</sub> nanoparticles through reaction of Zr(*n*-PrO)<sub>4</sub> with H<sub>3</sub>BO<sub>3</sub> and carbon has been studied with different ligands by carbothermal reduction at 1500 °C. In the first step, by introducing *N, N'*-bis (salicylidene)-1,3-diaminopropane (H<sub>2</sub>salpn) or salicylaldehyde (Hsal) species into reaction mixture, the reaction of the zirconium alkoxide using citric acid and boric acid yielded the zirconium diboride (ZrB<sub>2</sub>) sol–gel precursors. In the second step, the mixture was heated by introducing the reactant compact into an argon furnace held at 1500 °C for 2 h to obtain the final pure phase ZrB<sub>2</sub> nanocrystallites with a diameter of about 50 nm. The kind of chelating agent used in the preparation of ZrB<sub>2</sub> nanoparticles plays the predominant role on the final product size. This demonstrates that the proper kind of donor atom and a very specific ligand structure are necessary for the reaction of Zr<sup>4+</sup> complexes.

**Keywords:** ZrB<sub>2</sub> Nanoparticles, Sol–Gel Precursor, Schiff-Base Compound, Synthesis.

## 1. INTRODUCTION

Zirconium diboride (ZrB<sub>2</sub>) is one of the most important members of a family of ultra-high-temperature ceramics (UHTCs) with high melting point (>3000 °C).<sup>1</sup> ZrB<sub>2</sub> has low density (6.12 g/cm<sup>3</sup>),<sup>2</sup> low cost, high thermal, electrical conductivity, and oxidation resistance.<sup>3</sup> Recently, because of their interesting properties, diborides based ultra-high temperature ceramics, such as ZrB<sub>2</sub> and HfB<sub>2</sub> have attracted considerable attention. ZrB<sub>2</sub> powder is one of the particulate materials used for many purposes. The combination of properties makes ZrB<sub>2</sub> attractive for high temperature applications, such as furnace elements.<sup>4</sup>

One common method used in ZrB<sub>2</sub> nanoparticle production is sol–gel reaction synthesis.<sup>5</sup> The sol–gel process is one of the leading techniques for producing nanostructures with different morphologies of ceramic materials.<sup>6</sup> The applicable method shows promising potential for control over particle size, high purity and desired chemical homogeneity at the nanometer level.<sup>7</sup> Controlling the size and size distribution of nanoparticles is still a challenging problem, though great progress has been made in this direction.<sup>8</sup> Previous reports reveal that the most preponderant strategies to achieve desired properties of ZrB<sub>2</sub> are

including particle size control without using Schiff base complexes. From the survey of past studies on the synthesis of ZrB<sub>2</sub> nanopowder, one may notice that the synthesis of uniform crystalline nanoparticles of ZrB<sub>2</sub> and the fine control of their size by ligands has not been attained. Recently, the effect of Schiff base compounds on the size and morphology of ZrB<sub>2</sub> nanoparticles has been reported.<sup>9,10</sup> However, it should be noted that the chemistry of chelate complexes of Schiff base ligands is widely used as analytical reagents since they allow simple and inexpensive preparation and the wide range of applications.<sup>11</sup> Thus it seems necessary to study in more details the basic mechanism for the formation of ZrB<sub>2</sub> particles by Schiff-base compounds, particularly in the nano-size range, in order to control the size of this nanomaterial with sufficient uniformity.

The stability of metal complexes as precursors depends both on the metal ion and the ligand. The coordination of the ligand at the surface of the metal is important since this could be a factor related to the shape and size of the particles.<sup>12</sup> The ligand field effect employed in the formation of coordinate compounds plays the obvious role in the stability of the complexes.<sup>13</sup> One of the salicylaldehyde-derived series is salpn ligand containing four binding sites (N and O), with the flexibility of 1,3-propylenediamine

\*Author to whom correspondence should be addressed.

backbone compared with tetradentate salen and salophen Schiff base ligands.<sup>14,15</sup> On the other hands, different carbon sources have been extensively used for synthesis of ZrB<sub>2</sub> nanoparticles. Until now, ZrB<sub>2</sub> nanostructures were fabricated with the different carbon source such as citric acid, carbon black, graphite<sup>16</sup> and phenolic resin.<sup>17</sup> Citric acid was employed as both a chelating agent and a carbon source in the present synthetic process which is a protective agent against particle growth. The citrate sol-gel process with the mixing of ions at the atomic scale affects the hydrolysis reactions, and finally leads to the formation of the phase pure crystalline nanoparticle.

The present study is an approach that focuses on the synthesis of ZrB<sub>2</sub> nanopowder by using the advantages of the sol-gel process such as its versatility and the possibility to obtain high purity materials, and study the influence of conditions (starting materials) on the characteristics of nanoparticles. The aim of this study is to produce Zr(IV)(salpn) and Zr(IV)(sal) complexes as precursors for the preparation of ZrB<sub>2</sub> to explore the influence of ligand on the ultimate structures. The conformational differences between these two kinds of complexes result in marked differences in the size of particles and different abilities to induce nanoparticle assembly.

## 2. EXPERIMENTAL SECTION

Zirconium *n*-propoxide (Aldrich), salicylaldehyde, dionized water, boric acid, citric acid, acetic acid and methanol were purchased from Merck. The production of tetradentate ligand *N,N'*-bis(salicylidene)-1,3-diaminopropane (H<sub>2</sub>salpn) was carried out by the reaction of salicylaldehyde with 1,3-propylenediamine as reported previously.<sup>18</sup>

The preparation of ZrB<sub>2</sub> nanopowder was carried out as follows: 0.02 mol of zirconium *n*-propoxide was added to 25 ml of methanol followed by 4 ml of dionized water and 0.01 mol of salicylaldehyde. This mixture was shaken well for a couple of minutes and then distinguished volumes of citric acid and boric acid/acetic acid were added to the sol, and mixed well until the solution became homogeneous for 3 h at 65 °C. During formation, temperature of the solution was constantly monitored with the help of a thermometer placed within the solution through a glass breaker. After drying at 120 °C for 3 h, the obtained precursor was heated in an alumina furnace to 1500 °C at argon atmosphere. The heating rate was maintained at 2 °C/min, and ZrB<sub>2</sub> nanoparticles were synthesized at 1500 °C for 2 h. The flow rate of argon gas was 100 L/min. The experimental procedure used to prepare ZrB<sub>2</sub> nanosized particles is illustrated in Figure 1. The synthesis methods of zirconium complexes were investigated in the same conditions of solvent, temperature and argon pressure, but H<sub>2</sub>salpn was used instead of Hsal to synthesize Zr(IV)(salpn) precursor. The ZrB<sub>2</sub> nanostructures synthesized by using sal and salpn were denoted as A and B samples, respectively.

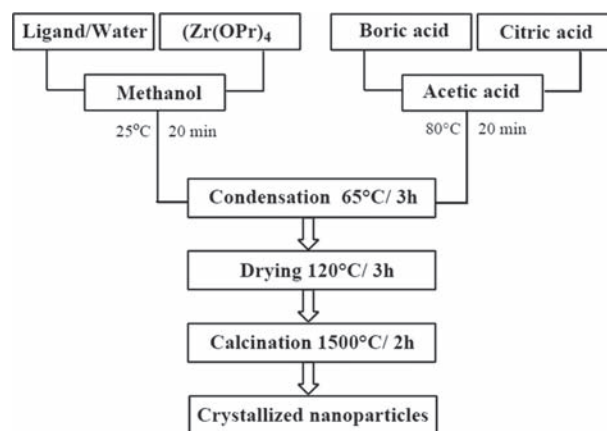


**Figure 1.** The schematic diagram of the sol-gel synthesis of ZrB<sub>2</sub> nanoparticles.

Different characterization methods were adopted to investigate the final particles. FT-IR spectra of compounds were recorded on Bruker-Tensor 27 spectrophotometer in the range of the 4000–400 cm<sup>-1</sup>. The microcapsule specimens were prepared by grinding the sample with potassium bromide (KBr). Thermogravimetric analysis (TG) and derivative thermogravimetry (DTG) were performed on a Linseys STA-1600 instrument under argon atmosphere from room temperature up to 1000 °C at a heating rate of 10 °C/min. X-ray powder diffraction analysis was conducted using a GNR.Co-Explorer with Cu-K $\alpha$  radiation and a step size of 0.02° (2 $\theta$ ). Data were digitally recorded in a continuous scan mode in the angle range of 20–70. Transition electron microscopy (TEM) observation was performed with a Philips-CM30 instrument, operating at 150 kV. Nanoparticles were prepared by placing a drop of the sample on a copper grid and allowing the ethanol to evaporate. Mira2 Tescan field emission scanning electron microscopy (FESEM) was used to image the size and morphology of the nanoparticle, and the specimens were coated with gold via sputtering.

## 3. RESULTS AND DISCUSSION

The zirconium diboride nanoparticle precursor was prepared by sol-gel methods, from Zr(IV) *n*-propoxide with the *in situ* one-step addition of boric acid (H<sub>3</sub>BO<sub>3</sub>) during the gelification process. The molar ratio of the carbon and boron to metal were 5 and 4, respectively. Zirconium *n*-propoxide was hydrolyzed in methanol with some water in a low-temperature synthesis (at 65 °C). The reactions can be carried out in the presence of Schiff-base compound and a controlled amount of water, and then crystalline nanoparticles can be synthesized conveniently at high temperatures.

The reaction of chelating agents with the zirconium alkoxide is an equilibrium reaction, and the identity of the species generated is sometimes difficult to predict. The stability of the sol strongly depends on the molecular

structure and type of atom in chelating agent. Differences in the structure of the chelating agents led to main effects on gelation time and condensation degree. The intermediate structures of precursors have been depicted to emphasize these differences (Fig. 2).

Hsal and H<sub>2</sub>salpn can be added to replace water in a chemical process. The zirconium atom has a different geometry with the N and O donor atoms coming from the tetra-dentate ligand (salpn) compared with an O donor atom of sal. The two nitrogen atoms and each phenoxo oxygen atom of the salpn ligand can bond to the zirconium(IV). The H<sub>2</sub>salpn ligand occupies the four equatorial positions, whereas the two propoxide ligands are trans-bonded. Nitrogen is less electronegative than oxygen and has a more available lone pair that led to a higher electron density at the zirconium atom, consequently higher inter-electronic repulsion by raising the energy of the d orbitals and less effective interaction with others. However, our results indicate that the N-donor ligand provokes a deformation of the Zr atom, which can be explained in terms of different hybridizations of the metal center that the N-donor ligand is less bulky than other types. The resulting sal ion becomes coordinated as a bidentate ligand to the zirconium(IV). In stoichiometric reaction an exchange of sal ion with the propoxy group in one molecule of zirconium(IV) is envisaged to occur. Prediction of coordination would place an O:O-coordinated sal ligand at a Zr(IV) site but would not be strict for the remaining groups. However, the ZrO<sub>2</sub> was firstly prepared, and secondly ZrB<sub>2</sub> powder was successfully synthesized via carbothermal reduction by boron and carbon sources.<sup>19</sup> The reactions showed that the carbothermal reduction of ZrO<sub>2</sub> with carbon could be completed with an excess of H<sub>3</sub>BO<sub>3</sub> to compensate the loss of B<sub>2</sub>O<sub>3</sub>. The B<sub>2</sub>O<sub>3</sub> product in during reaction played an important role in synthesizing ZrB<sub>2</sub>. In fact, B<sub>2</sub>O<sub>3</sub> has a low melting point about 450 °C, that a rapid vaporization is obtained at temperatures above 1100 °C.<sup>20</sup> B<sub>2</sub>O<sub>3</sub> and ZrO<sub>2</sub> tended to react with carbon to form ZrB<sub>2</sub>.<sup>16,19</sup> The amount of carbon is dictated by the decomposition of citric acid with three moles of C. During the heat-treatment process, a great deal of gases including CO as an efficient reducing agent was produced and escaped away. Finally, a single phase of ZrB<sub>2</sub> without residual ZrO<sub>2</sub> was achieved at 1500 °C.

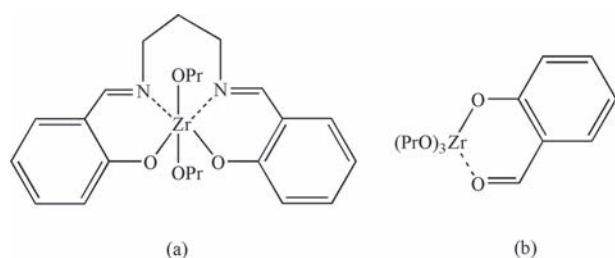


**Figure 2.** The structure of zirconium complexes obtained from H<sub>2</sub>salpn (a) and Hsal (b).

The process of calcination of the dried gel was studied by thermal analysis (TG-DTG) of two samples. Two precursor powders behave similarly, since the citric acid and boric acid quantity are the same and the peaks corresponding to ligand completely overlap with together in both samples. Figure 3 shows that the main weight loss occurs below 500 °C, and the total mass loss of the samples was 67.5%. The subdivision of the carbothermal reduction of ZrB<sub>2</sub> in some reaction steps is clearly demonstrated by the results of direct monitoring by DTG. The curve shows a process about 100 °C which takes place with low speed. This can likely due to water elimination and decomposition of boric acid. A single peak with significant intensity between 170 and 260 °C was observed that appeared to be due to the initiation of citric acid decomposition. As shown

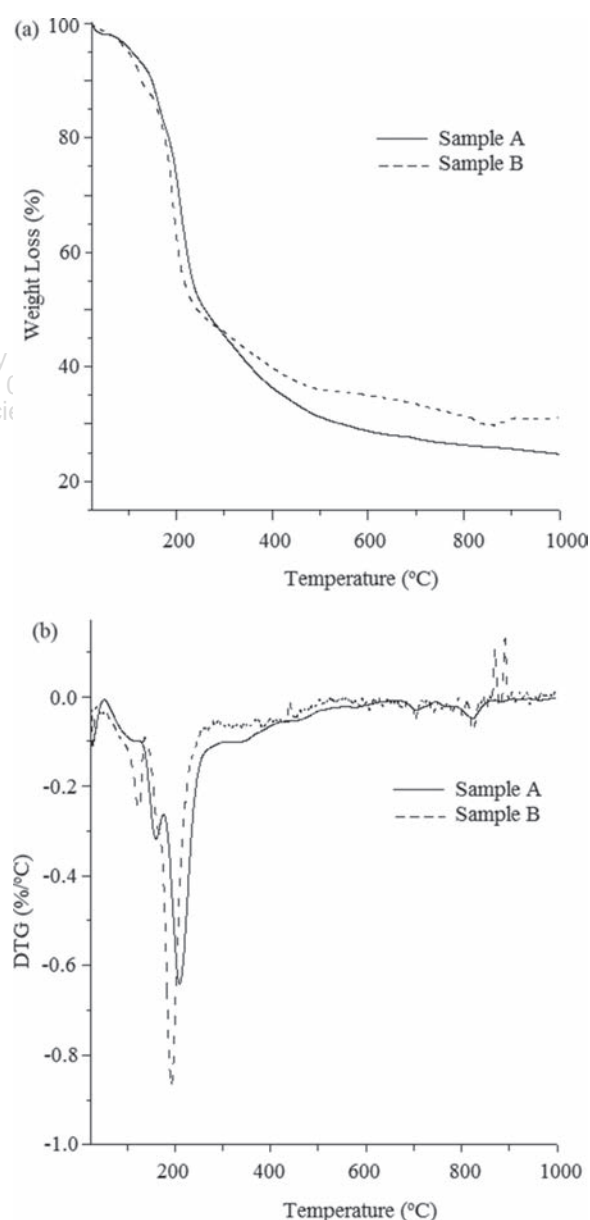


**Figure 3.** TG-DTG curve of calcination process for sample B.

in DTG curve, decomposition of citric acid is a single-step process,<sup>21</sup> also confirmed by the mass losses indicated on the TG curve. At 800 °C to 900 °C, the thermal interactions of ZrO<sub>2</sub> occurred, and when the temperature was 1200 °C, ZrO<sub>2</sub> reacted with B<sub>2</sub>O<sub>3</sub> that the weight loss accelerated again and tended to stabilize, which is believed to be the process of the carbothermal reduction reaction.

Both ZrB<sub>2</sub> precursor particles prepared via sol-gel method were characterized by FTIR analysis primarily. Figure 4 shows the FTIR spectra of the powders produced at 120 °C. The very strong absorption at 3260 cm<sup>-1</sup> and the weak peak at 1650 cm<sup>-1</sup> are in the range for the absorption band of O-H stretching and bending vibrations, respectively. It is obvious that this spectrum exhibits peaks at 1197, 1470 cm<sup>-1</sup> and another small peak at 1633 cm<sup>-1</sup>, implying the presence of the phenolic C-O, C=C and C=N in the Schiff base ligand (salpn), respectively.<sup>18</sup> However, another small band located at 930–710 cm<sup>-1</sup> (asymmetric stretching) and a band at 1190 cm<sup>-1</sup> (B-OH bending) are in the range for the absorption band of B-O-H.<sup>14</sup>

XRD patterns of the powders calcined at 1500 °C show the characteristic XRD peaks of single phase zirconium diboride in Figure 5. It is evident that no obvious Bragg diffraction peaks have been detected in the precursor, as shown in Figure 5(a), indicating that the sample is amorphous in structure. Figures 5(b) and (c) display the XRD spectrum of sample A and B, respectively. The resulting materials from both processes can be identified the crystal structure of ZrB<sub>2</sub> that is hexagonal. If sufficient carbon was provided, this would logically result in only zirconium diboride without carbide and oxide after carbothermal reaction. In a stoichiometric reaction, the gel required 5C/Zr for the carbothermal reduction. According to the absence of any peak corresponding to ZrO<sub>2</sub> and ZrC in the XRD pattern of both samples,<sup>22</sup> a conclusion can be drawn that the carbothermal reduction of two samples has

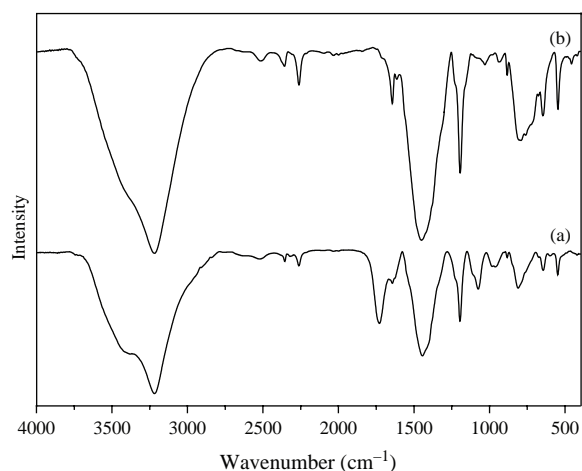


**Figure 4.** FTIR spectra of the ZrB<sub>2</sub> precursors for synthesis of (a) sample A and (b) sample B.

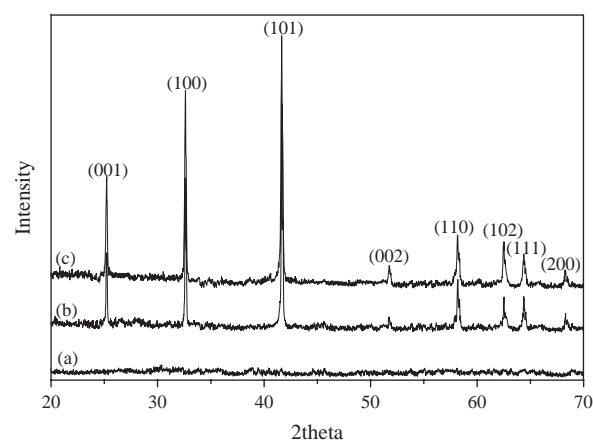


**Figure 5.** XRD patterns of (a) precursor, (b) sample A and (c) sample B.

been completed at 1500 °C for 2 h, and the molar ratios of C and B in the pyrolyzed gel were sufficient to ZrB<sub>2</sub> synthesis.

The produced nanopowders were visualized by field emission scanning electron microscopy. The effect of ligand on particle size is clearly observed in FESEM images (Fig. 6). With adding sal compared to salpn, the aspect ratio of the particles was increased, but the particles were not agglomerated in Figure 6(a). Conversely, salpn ligand led to produce smaller nanoparticles, but they having practically nonuniformity diameters are not clearly distinguishable, and appear to adhere to each other as shown in Figure 6(b). Nitrogen is less electronegative than oxygen, and it has a more available lone pair, one might guess a higher electron density at the zirconium atom. Hence, the nitrogen interaction is strong enough to make breakdown of the crystal structure. This molecular geometry of the H<sub>2</sub>salpn is in relation to the smaller size of crystalline nanoparticles that are embedded in a glassy phase. On the other hands, Hsal produces chelating species that they are different compared with H<sub>2</sub>salpn. The reaction of sal ion involved the interaction of two O groups with Zr ions and complexation, which formed a complex through a Zr atom binding to O atoms.

Figures 7(a) and (b) show typical TEM images of sample A and B, respectively. It indicates that the particles

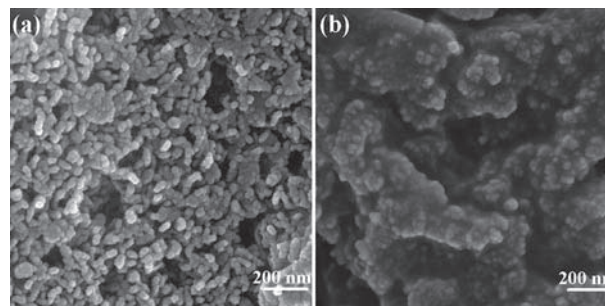


**Figure 6.** FESEM micrographs of (a) sample A and (b) sample B.

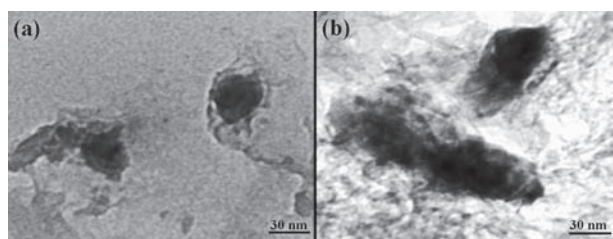


**Figure 7.** TEM micrographs of (a) sample A and (b) sample B.

are nearly spherical (Fig. 7(a)), and the average particle size is 30 nm. A variable distribution of particle size is clearly observed in Figure 7(b), showing the different form of nanoscale particles in sample B. It is interesting to note that Schiff-base compounds play the role of a stabilizer of Zr(IV) ion against hydrolysis. The rate-determining step for the formation of ZrB<sub>2</sub> can be due to the inhibition of the nucleation or the growth of the generated particles by the adsorption of ligand thereon.<sup>23</sup> Accordingly, the particle-size distribution of ZrB<sub>2</sub> indicated that the average diameter of nanoparticles counted from the TEM image is about 30–50 nm. Such investigations can increase our knowledge on synthesis of refractory and hard materials, and offer a guide for controlling the structure of the products.

Thus, Zr(IV)(sal) complex is selected as desired precursor after the observation of microstructure of synthesized ZrB<sub>2</sub> nanopowders. The slower growth rate may be due to the versatile structure of the salpn and interaction between the zirconium ion and nitrogen atoms of the amine groups.<sup>24,25</sup> Anyway, it can be obvious that the observed reaction pathway depends on the chemical functionality of the incoming compounds.

#### 4. CONCLUSIONS

Synthesis of ZrB<sub>2</sub> nanoparticles by sol–gel process has proved to be very efficient in controlling the size of the particles obtained from the ligands derived from salicylaldehyde. In this synthesis, investigations on reaction mechanisms are necessary for processing optimization to improve the properties of the products. The zirconium ion is coordinated through the azomethine (salpn) nitrogens and phenolic oxygen atoms that the nitrogen donor group of salpn ligand leads to the unusual properties of nanoparticles, which should be taken careful consideration of the metal-salpn complexes. From these results, we can conclude that Zr(IV)(sal) complex could be used for controlling smaller size of particles with excellent

uniformity compared with other literatures. According to SEM images, it was observed that ligand plays a key role in controlling the growth of ZrB<sub>2</sub> nanostructures as well as providing an in depth understanding of Zr(IV) complexes and how ligand work.

**Acknowledgments:** The authors are grateful to the Space Transportation Research Institute of Iran for financial support.

#### References and Notes

1. Y. Xie, T. H. Sanders Jr., and R. F. Speyerw, *J. Am. Ceram. Soc.* 91, 1469 (2008).
2. H. Wang, X. Chen, B. Gao, J. Wang, Y. Wang, S. Chen, and Y. Gou, *Appl. Organometal. Chem.* 27, 79 (2013).
3. S. E. Kravchenko, V. I. Torbov, and S. P. Shilkin, *Russ. J. Inorg. Chem.* 56, 506 (2011).
4. S. Guo, C. Hu, and Y. Kagawa, *J. Am. Ceram. Soc.* 94, 3643 (2011).
5. L. S. Walker and E. L. Corral, *J. Am. Ceram. Soc.* 97, 399 (2014).
6. D. H. Chen and X. R. He, *Mater. Res. Bull.* 36, 1369 (2001).
7. Y. Yan, Z. Huang, X. Liu, and D. Jiang, *J. Sol–Gel Sci. Technol.* 44, 81 (2007).
8. P. Sahu and B. L. V. Prasad, *Nanoscale* 5, 1768 (2013).
9. R. Li, Y. Zhang, H. Lou, J. Li, and Z. Feng, *J. Sol–Gel Sci. Technol.* 58, 580 (2011).
10. H. Ji, M. Yang, M. Li, G. Ji, H. Fan, and X. Sun, *Adv. Powder Technol.* 25, 910 (2014).
11. J. Welby, L. N. Rusere, J. M. Tanski, and L. A. Tyler, *Inorg. Chim. Acta* 362, 1405 (2009).
12. L. K. Sannegowda, K. R. Venugopala Reddy, and K. H. Shivaprasad, *RSC Adv.* 4, 11367 (2014).
13. R. B. Grubbs, *Polym. Rev.* 47, 197 (2007).
14. M. R. Maurya, S. J. J. Titinchi, S. Chand, and I. M. Mishra, *J. Mol. Catal. A: Chem.* 180, 201 (2002).
15. S. J. Dzigan and V. L. Goedken, *Inorg. Chem.* 25, 2858 (1986).
16. H. Qiu, W. Guo, J. Zou, and G. Zhang, *Powder Technol.* 217, 462 (2012).
17. Y. Yan, Z. Huang, S. Dong, and D. Jiang, *J. Am. Ceram. Soc.* 89, 3585 (2006).
18. M. Salavati-Niasari, B. Shoshtari-Yeganeh, and F. Mohandes, *Mater. Res. Bull.* 48, 1745 (2013).
19. D. D. Lee, G. D. Sim, K. Xiao, and J. J. Vlassak, *J. Phys. Chem. C* 118, 21192 (2014).
20. A. Paul, S. Venugopal, J. G. P. Binner, B. Vaidhyanathan, A. C. J. Heaton, and P. M. Brown, *J. Eur. Ceram. Soc.* 33, 423 (2013).
21. D. Wyrzykowski, E. Hebanowska, G. Nowak-Wicz, M. Makowski, and L. Chmurzynski, *J. Therm. Anal. Calorim.* 104, 731 (2011).
22. R. V. Krishnaraon, M. Z. Alam, D. Kumar Das, and V. V. Bhanu Prasad, *Ceram. Int.* 40, 15647 (2014).
23. J. H. Son, S. W. Kim, D. S. Bae, K. S. Han, J. K. Lee, C. Y. Kim, B. I. Kim, and J. H. Adair, *Mater. Sci. Eng. A* 498, 2 (2008).
24. M. Salehi, M. Kubicki, G. Dutkiewicz, A. Rezaei, M. Behzad, and S. Etminani, *Russ. J. Coord. Chem.* 39, 716 (2013).
25. P. Adaó, J. Costa Pessoa, R. T. Henriques, M. L. Kuznetsov, F. Avecilla, M. R. Maurya, U. Kumar, and I. Correia, *Inorg. Chem.* 48, 3542 (2009).

Received: 15 October 2014. Accepted: 6 February 2015.